Effective Mass Determination in Highly Resistive GaAs by Exploiting the Influence of a Magnetic Field on Optically Excited Transient THz Surface Emissions

G. Chen,[1,2] D. Chakraborty,[1,2] J. Cheng,[1,2] M. Mikulics,[3] C. Chimera,[4] I. Komissarov,[4] R. Adam,[5] D. E. Bürgler,[5] C. M. Schneider,[5,6] H. Hardtdegen,[3] and R. Sobolewski[1,2,4]

[1]Laboratory for Laser Energetics, University of Rochester
[2]Materials Science Graduate Program, University of Rochester
[3]Research Centre Jülich, Ernst Ruska Centre for Microscopy and Spectroscopy with Electrons, Germany
[4]Department of Electrical and Computer Engineering, University of Rochester
[5]Research Centre Jülich, Peter Grünberg Institute (PGI-6), Germany
[6]Department of Physics, University of California Davis

Generating broadband, free-space terahertz transients by pumping the surface of a semiconductor with femtosecond optical laser pulses is a well-established technique, generally called THz surface emission.[1] Several radiation models have been proposed to explain the THz surface emission such as surface depletion created by the internal electric field perpendicular to the sample surface,[2–5] nonlinear optical rectification,[6,7] and photocurrent generated by the photo-Dember effect.[8–10] It was also demonstrated that an external magnetic field applied in the plane of a semiconductor can tune the amplitude of the surface-emitted THz radiation. The enhancement of the THz amplitude was ascribed to the Lorentz force, induced by the applied magnetic field, which introduced an additional acceleration to the photocarriers.[11,12] Time-domain, nonequilibrium carrier relaxation dynamics can be characterized by an optical pump–probe spectroscopy technique,[13] which allows one to further analyze how the Lorentz force affects photocarriers and to determine the relationship between the THz transient amplitude enhancement and the semiconductor carrier mobility.

For these studies, five different, highly resistive (111)-oriented GaAs samples characterized by different mobilities and crystalline conditions were used. Namely, a standard semi-insulating GaAs wafer (SI GaAs), a semi-insulating GaAs wafer annealed at 300°C (annealed GaAs), and three nitrogen-ion–implanted GaAs specimens, implanted at an energy of 191 keV with a dose of $\sim 8 \times 10^{11}$ ions/cm^2 (Refs. 14 and 15), and, subsequently, annealed at 300°C, 350°C, and 400°C, denoted as N-GaAs 300, N-GaAs 350, and N-GaAs 400, respectively.

Experiments were performed using THz time-domain spectroscopy (THz-TDS) and optical femtosecond pump–probe spectroscopy (F-PPS). In both cases, a commercial Ti:sapphire laser that generated a train of nominal, 100-fs-wide laser pulses at 800-nm wavelength and 76-MHz repetition rate was used. In the THz-TDS setup,[16] the laser beam was split into two branches with a 90:10 power ratio. The high-power branch, after bouncing from a retroreflector mounted on a delay stage, was focused on our test GaAs sample to generate bursts of electromagnetic radiation, i.e., single-picosecond transients with the frequency spectrum extending into THz, while the low-power branch was used for the THz transient detection and focused on a commercial low-temperature–grown GaAs photoconductive (PC) THz detector with z-axis polarization sensitivity (perpendicular to the optical table).[17] A 5-mm-diam and ~10-mm-focal-length Teflon™ (polytetrafluoroethylene) lens, located between the test sample and the THz detector, collimated the transmitted THz radiation. In addition, an external magnetic field **B** was applied in the sample plane along the x axis, while the surface-emitted THz radiation was collected along the y direction, as indicated in Fig. 1. The F-PPS system was implemented to measure the nonequilibrium carrier dynamics in the samples. In this setup[18,19] optical pulses were split into two beams by a 60/40 beam splitter. Pump pulses had the higher power, and the beam was modulated with an acousto-optic modulator. The lower-power probe beam was delayed with respect to the pump by reflection from a retroreflector

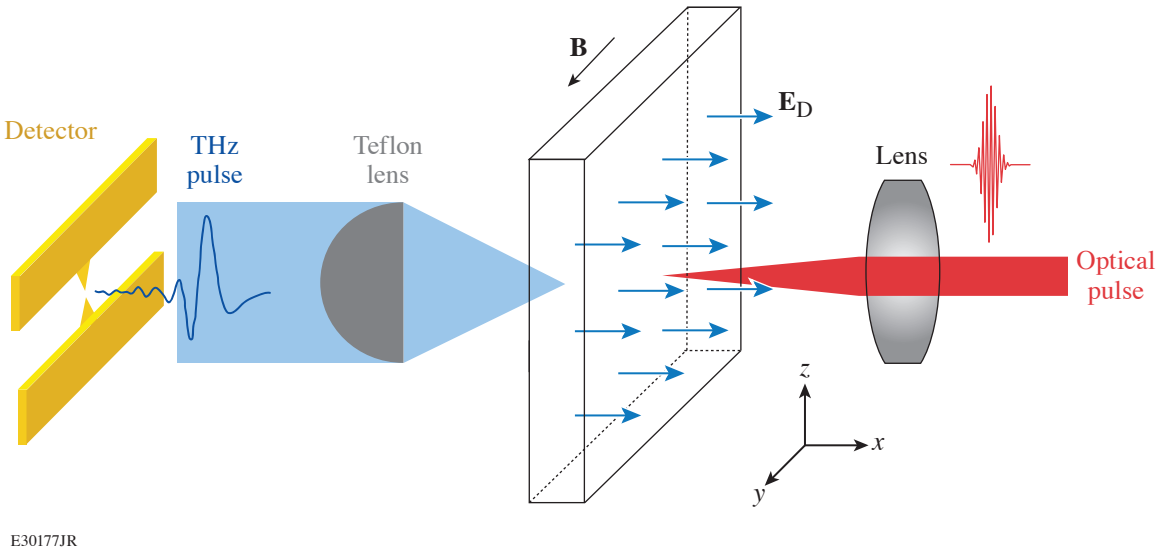

Figure 1
Schematics of the basic experimental geometry. The surface of the sample is parallel to the x–z plane. The built-in depletion electric field $\mathbf{E}_D$ is along the y axis and perpendicular to the sample surface. A lens is used to focus a laser beam at the surface of the sample, and a Teflon lens placed after the sample collimates the emitted THz radiation toward a PC THz detector aligned in such a way that it can only sense the z component of the THz transient. An external magnetic field applied along the x axis was used in the **B**-field enhancement experiments.

mounted on a delay stage. Both pump and probe beams were focused on the same spot of the sample; the beam size of the probe (~20 μm in diameter) was kept slightly smaller than that of the pump beam (~30 μm in diameter) to ensure probing only the optically excited area of the sample. To limit the probe-related electron heating to a minimum and to ensure a decent signal-to-noise ratio, the power ratio of the pump to probe beams was set to ~10:1. The probe beam was reflected at the sample surface and directed toward a photodetector connected to a lock-in amplifier to record the normalized reflectivity change ($\Delta R/R$) waveforms as a function of the time delay between the pump and probe pulses.

Figure 2 shows the dependence $k = (q/m^*)\tau_1$, where q is the elementary charge, m^* is the electron effective mass, and τ_1 is the relaxation time, for all five types of GaAs samples (black circles) and reveals a universal linear relationship (black solid line). This indicates that τ_1, derived based on the Drude model, is the trapping time for the samples. During this time, the Lorentz force accelerates electrons before they get trapped by defect states. Therefore, a high density of defects/traps in a semiconductor, e.g., in case of the N-GaAs samples, leads to a shorter carrier lifetime, which, in turn, limits the impact of the magnetic field on the THz transient.

The next important conclusion from Fig. 2 is that within the linear fit, the effective mass $m^* = q/(k/\tau_1)$ for all samples is exactly the same and the extracted value is $m^*/m_0 = 0.059$ (m_0 is the electron mass), which is close to the accepted value of 0.063 for GaAs single crystals,[20] and illustrated by the dashed line corresponding to the k dependence for $m^*/m_0 = 0.063$. The latter is an interesting result and shows that despite the large differences in the crystallinity of the test samples, the effective mass derived from our magnetic-field experiments remains constant and very close to the effective mass of electrons in GaAs with a perfect crystalline structure. The only deviation from the ideal m^* value observed was for the annealed GaAs sample. Contrary to the other samples, the clear distinction between trapping and recombination processes is somewhat difficult to establish.

In conclusion, we exhaustively analyzed the transient emission of THz signals, emitted from highly resistive GaAs samples with different crystallinity, excited by femtosecond optical pulses. The observed magnetic field impacted the THz transient generation, and the corresponding enhancement factor was directly proportional to the applied **B** field. Interestingly, the slope of the enhancement factor dependence was directly proportional to the samples' nonequilibrium trapping time measured using

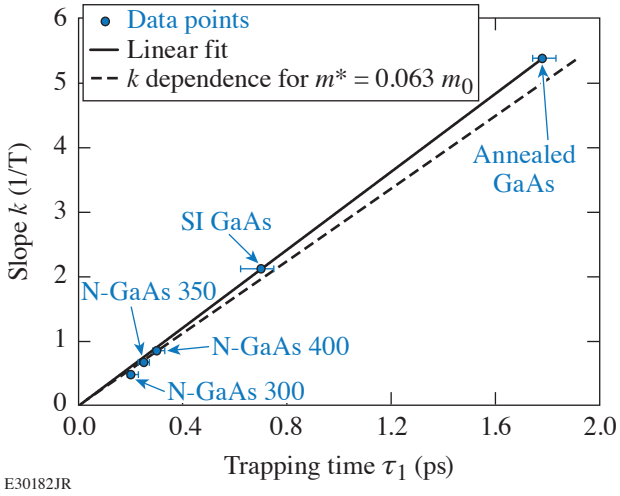

Figure 2
Dependence of the slope k on the trapping time τ_1. The circles are experimental data, and the black line is the best linear fit yielding $m^*/m_0 = 0.059$. The dashed line corresponds to the k dependence for the literature $m^*/m_0 = 0.063$.

femtosecond optical pump–probe spectroscopy. The latter enabled the determination of the electron effective mass $m^*/m_0 = 0.059$ that was very close to the literature m^* value for GaAs single crystals. The latter reveals that GaAs samples with very different crystallinity, including highly defected, N-implanted samples, all have an m^* value essentially equal to that of the ideal crystal.

This material is based upon work that was supported in Rochester in part by the National Science Foundation Grant Number 1842712. The work at the Research Center Jülich was performed within JuSPARC (Jülich Short-pulse Particle Acceleration and Radiation Center), a strategy project funded by the Federal Ministry of Education and Research (Bundesministerium für Bildung und Forschung).

1. X.-C. Zhang *et al.*, Appl. Phys. Lett. **56**, 1011 (1990).
2. X.-C. Zhang and D. H. Auston, J. Appl. Phys. **71**, 326 (1992).
3. R. Kersting *et al.*, Phys. Rev. B **58**, 4553 (1998).
4. J. N. Heyman *et al.*, Phys. Rev. B **64**, 085202 (2001).
5. J. S. Hwang *et al.*, Appl. Phys. Lett. **87**, 121107 (2005).
6. S. L. Chuang *et al.*, Phys. Rev. Lett. **68**, 102 (1992).
7. M. Reid, I. V. Cravetchi, and R. Fedosejevs, Phys. Rev. B **72**, 035201 (2005).
8. K. Liu *et al.*, Phys. Rev. B **73**, 155330 (2006).
9. R. Mendis *et al.*, J. Appl. Phys. **98**, 126104 (2005).
10. A. Reklaitis, J. Appl. Phys. **108**, 053102 (2010).
11. X.-C. Zhang *et al.*, Appl. Phys. Lett. **62**, 2003 (1993).
12. C. Weiss, R. Wallenstein, and R. Beigang, Appl. Phys. Lett. **77**, 4160 (2000).
13. A. Othonos, J. Appl. Phys. **83**, 1789 (1998); **84**, 1708(E) (1998).
14. M. Mikulics *et al.*, Appl. Phys. Lett. **87**, 041106 (2005).
15. M. Mikulics *et al.*, Appl. Phys. Lett. **88**, 041118 (2006).
16. R. Adam *et al.*, Appl. Phys. Lett. **114**, 212405 (2019).
17. A. Geižutis *et al.*, Opt. Mater. **30**, 786 (2008).
18. J. Zhang *et al.*, J. Appl. Phys. **110**, 113112 (2011).
19. J. Serafini *et al.*, Semicond. Sci. Technol. **31**, 045006 (2016).
20. G. Margaritondo, in *Encyclopedia of Condensed Matter Physics*, edited by F. Bassani, G. L. Liedl, and P. Wyder (Elsevier, Oxford, 2005), pp. 311–321.